International Journal of Engineering and Geosciences
https://dergipark.org.tr/en/pub/ijeg
e-ISSN 2548-0960

A Comparative Analysis of Machine Learning Techniques for LULC Classification Using Landsat-8 Satellite Imagery

Pratibha P. Dapke [*1], Syed Ahteshamuddin Quadri [1], Samadhan M. Nagare [1], Sagar B. Bandal [1], Manasi R. Baheti [1]

[1] *Dr. Babasaheb Ambedkar Marathwada University, Department of CS and IT, India, pratibhadapke189@gmail.com syedahtesham1432@gmail.com, samadhannagre340@gmail.com,sagarbandal2901@gmail.com,mrb.csit@bamu.ac.in*

Cite this study: Dapke, P., Syed, A., Nagare, S., Bandal, S., & Baheti, M. (2025). A Comparative Analysis of Machine Learning Techniques for LULC Classification Using Landsat-8 Satellite Imagery. International Journal of Engineering and Geosciences, 10 (1), page numbers.

https://doi.org/10.26833/ijeg.1503104

Keywords
Remote Sensing
GIS
Landsat-8 Imagery
LULC
Machine Learning Algorithm

Research/Review Article

Received:
Revised:
Accepted:
Published:

Abstract

This study compares various classification methods to assign land use land cover (LULC) classes. Using Geographic Information Systems (GIS) and Remote Sensing (RS) to leverage the dynamic and complex area of LULC, this study examines the potential of different machine learning classification methods. Precise differentiation and classification of various land cover categories, such as green vegetation, urban areas, water bodies, dark green vegetation, and bare terrain, are made possible by the high spatial and spectral resolution of Landsat imagery. For efficient land management and planning, the integration of Landsat data with GIS and RS approaches provides insightful information about the distribution and temporal changes in LULC. This study uses four classifiers to explore the fundamentals of supervised machine learning techniques and identify their drawbacks and advantages. Testing results show that the Support Vector Machine with four kernels- linear (99.17%), radial basis (RBF) (99.11%), sigmoid (99.11%), and polynomial (99.11%) is a reliable option for LULC classification, outperforming other classifiers in terms of accuracy, including the Minimum Distance Classifier (MDC-93.47%), Maximum Likelihood Classifier (MLC-98.98%), and Mahalanobis Distance Classifier (MHC-97.83%). Among the tested classifiers, Support Vector Machine with four kernels notably shows the highest accuracy. With their essential insights for well-informed decision-making towards sustainable development and resource utilization, our findings add to a thorough understanding of LULC dynamics. For accurate mapping and long-term monitoring of deviations in LC, the study emphasizes the value of using advanced classification systems in remote sensing applications. This study compares several classification methods to assign Land Use Land Cover (LULC) classes using Landsat-8 imagery from September 2022. Although this research focuses on a single time point, the resulting LULC map provides insights into the spatial distribution of human activities such as urbanization and agricultural expansion. The findings serve as a foundation for future studies that will incorporate time series data to detect temporal changes in land cover. This information is crucial for promoting sustainable land management practices in the study area.

1. Introduction

LULC analysis is an essential part of natural resource management, land-use planning, and environmental monitoring programs around the globe [1]. The rapid expansion of human activities and urbanization has led to significant changes in LC patterns, necessitating accurate and timely monitoring techniques. The utilization of satellite images in particular has made remote sensing an effective means of recording the geographical and temporal dynamics of land cover changes. Landsat-8, launched by NASA and the USGS in 2013, offers high-resolution multispectral imagery with a revisit time of 16 days, making it an invaluable resource for LULC analysis [2].

The utilization of Landsat-8 data for LULC analysis presents numerous advantages, including its moderate spatial resolution (30 meters), which strikes a balance between detail and coverage, and its multi-temporal capabilities, allowing for the detection of seasonal and long-term changes. Furthermore, Landsat-8 data are

freely available, enabling widespread access and facilitating large-scale studies across diverse geographical regions [3]. Leveraging these advantages, researchers have employed Landsat-8 imagery to investigate various land cover dynamics, including urban expansion, deforestation, agricultural intensification, and ecosystem monitoring [4].

The implication of this research is that it is possible to enhance our consideration of LULC dynamics and inform evidence-based administrative in environmental management and land-use planning [5].

Ultimately, the study's findings are expected to contribute valuable insights to the broader scientific community and facilitate the development of effective strategies for mitigating environmental degradation and promoting ecosystem resilience considering the state of the world today [6].

Remote sensing and GIS technologies have revolutionized the study of LCLU changes, offering unprecedented capabilities in spatial data collection, storage, analysis, and visualization. These tools provide a flexible framework for detecting variations in LC over time, primarily driven by the availability of remote sensing imagery and the analytical prowess of machine learning algorithms [7]. The abstraction of LULC data from such imagery relies on discerning spectral, textural, geometric, and contextual properties embedded within the images. This information serves as the foundation for creating maps essential in diverse fields such as urban planning, environmental conservation, disaster management, and infrastructure development [8].

2. LITERATURE REVIEW

The effectiveness of machine learning methods in LULC classification has been compared in a number of studies. For example, using Landsat-8 images, machine learning algorithms like Random Forest (RF), Support Vector Machines, and artificial neural networks (ANN) achieved good accuracy in categorizing LULC types, according to a study focused on the Dehradun region in India. [9-10].

An object-oriented approach using time series Landsat-8 images has been proposed for more accurate LULC mapping. This method involves segmenting images into meaningful objects and then classifying them, which has been shown to reduce misclassification compared to traditional pixel-based methods [11].

Studies have also examined how LULC alterations affect the ecosystem. For example, studies in various regions have assessed how changes in land use and land cover influence hydrology, biodiversity, and ecosystem services, using Landsat-8 data to track these changes and model their future impacts [11].

The utilization of cloud-based platforms like Google Earth Engine (GEE) has facilitated large-scale LULC mapping and analysis. Studies leveraging GEE have demonstrated its capability to process large datasets efficiently, enabling the monitoring of LULC changes over time with high accuracy [10].

Research has shown the benefits of integrating Landsat-8 data with other satellite data, such as Sentinel-2. This combination improves classification accuracy, especially in heterogeneous and urban environments. For example, one study evaluated Landsat-8, Landsat-9, and Sentinel-2 imagery for LULC classification in urban areas, highlighting the complementary strengths of each dataset [11].

This research provides a thorough examination of the function of remote sensing and GIS technologies in detecting changes in land use and land cover. We highlight the importance of machine learning classifiers in improving the precision and effectiveness of categorization. Through empirical evaluation and comparison of classification methodologies [12]. This research contributes to advancing our understanding of effective approaches for characterizing LULC changes, enabling well-informed decision-making in sustainable development and land management initiatives.

The importance of this study to analysis using remote sensed data in a selected study area lies in its ability to provide critical insights for environmental management, urban and regional planning, and agricultural optimization. It supports disaster preparedness, water resource management, and infrastructure development by identifying land use patterns and changes. LULC analysis aids in achieving Sustainable Development Goals (SDGs), fostering economic growth, and preserving cultural sites, thereby enabling informed decision-making and sustainable development for the area's overall well-being.

This paper is to do a comprehensive analysis of LULC dynamics using Landsat-8 data and machine learning techniques. By using advanced classification algorithms with Landsat-8 imagery, the study seeks to elucidate the spatial patterns of land cover changes over a selected study area. The research will employ a range of machine learning classifiers and four classification methods to accurately classify land cover classes based on spatial, spectral, and temporal information extracted from Landsat-8 imagery.

The objective of this study is to compare classification methods for assigning LULC classes using Landsat-8 imagery. The LULC map produced serves as a tool to evaluate the influence of human activities, such as urban expansion and deforestation, on natural ecosystems. While the study focuses on the 2022 data, the insights gained will aid in future work on change detection and sustainable land management by identifying key areas of concern. The results will support policymakers and land managers in making data-driven decisions.

In this study, the research workflow is, 1. Use Landsat-8 data to classify five different land cover types. 2. Assess the land cover classification's correctness results by comparing them against ground-truth data or higher-resolution imagery. 3. Examine the spatial distribution of land use and land cover across the study area to understand landscape patterns and spatial heterogeneity.

3. STUDY AREA

This study focuses on the socioeconomic dynamics of Sillod taluka, which is located in the India, Marathwada region of Maharashtra, Aurangabad district. Sillod Taluka is in the Aurangabad Division's administrative authority

and is situated in the northeastern section of the Aurangabad city. At latitude 19.88 and longitude 75.34 are its coordinates. A 33-degree bearing points in the direction of Sillod from Aurangabad. At this juncture, the height is 330 meters above sea level.

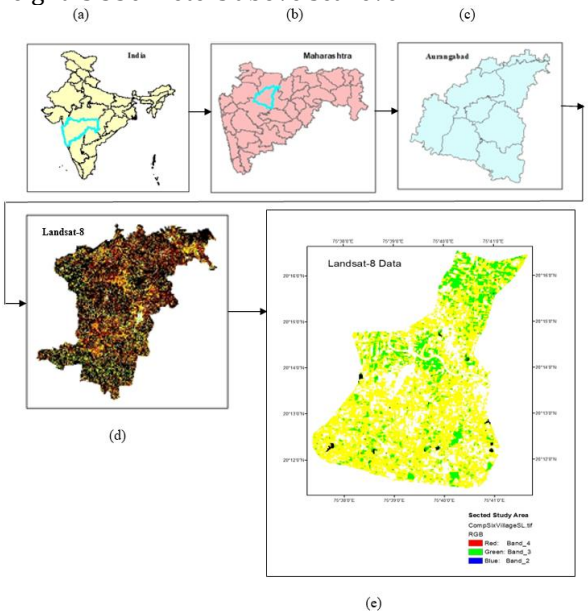

Figure 1. (a) India, (b) Maharashtra, (c)Aurangabad, (d)Landsat-8 Data, (e)Selected Study Area using Landsat-8 Image.

4. METHODS

In this study, land use land cover, the research process involves several key steps, starting with defining the study's objectives, such as monitoring urban growth or assessing environmental changes, then collecting remote sensing Landsat-8 satellite data and preprocessing it through georeferencing, radiometric corrections, and image enhancement. The data is classified using techniques such as supervised classification methods. Classification accuracy is assessed against ground truth data. Post-classification processing, including smoothing, refines the results. To analysis like machine learning algorithms, i.e., SVM, MLC, MDC, and MHC, the accuracy and depth of insights. Integrating these findings with GIS data further supports environmental monitoring, urban planning, and sustainable development efforts.

4.1 Remote sensing data and preprocessing

The imagery consisted of 2022 Landsat-8 satellite images, including OLI (Operational Land Imager). Geometric correction and L1T (level 1T) acquisition were applied to every image [13]. They were downloaded for free from the USGS website but sourced through the Google Earth Engine [14-15]. The image was taken last week of September 2022, since many types of vegetation are in a stable stage at this time of year. Table 1. shows the database and its sources.

11 spectral bands are seen in this image. Table 2. provides further acquisition parameters of Lansat-8 imagery. As a result, the high spatial, temporal, and spectral resolution of sentinel satellites is suitable for LULC monitoring missions.

including Landsat 8, capture images across multiple wavelengths (or spectral bands) of the electromagnetic spectrum. Each of these bands records data at different portions of the spectrum, such as visible light, near-infrared, shortwave infrared, and thermal infrared, which allows for detailed analysis of various surface features and phenomena on Earth [16-17].

Table 1. Shows the Database and its sources.

Sr. No.	Dataset	Apparatus Sensor	Source
	Landsat-8	Operational Land Imager (OLI)	https://earthexplorer.usgs.gov/

Table 2. Spectral Band Description.

Spectral Band	Spectral Range	Resolution
Band 1	Coastal Aerosol-0.43 - 0.45 µm	30 m
Band 2	Blue -0.450 - 0.51 µm	30 m
Band 3	Green -0.53 - 0.59 µm	30 m
Band 4	Red -0.64 - 0.67 µm	30 m
Band 5	Near-Infrared - 0.85 - 0.88 µm	30 m
Band 6	SWIR 1-1.57 - 1.65 µm	30 m
Band 7	SWIR 2 - 2.11 - 2.29 µm	30 m
Band 8	Panchromatic (PAN) - 0.50 - 0.68 µm	15 m
Band 9	Cirrus -1.36 - 1.38 µm	30 m
Band 10	TIRS 1 - 10.6 - 11.19 µm	100 m
Band 11	TIRS 2 - 11.5 - 12.51 µm	100 m

ArcGIS 10.8.2 [18] The Dark Object Subtraction (DOS) technique [19] was used to apply atmospheric correction through [20]. The suggested methodology was validated using field data and a Google Earth image [21-22]. Ground control points (GPSs) [23]. were used in the field to conduct surveys of ground truth. The cloud cover is 0.01 of Landsat-8 data. Furthermore, baseline information was acquired based on an official map of the research area's forest stand, in addition to earlier information and detailed discussions with stakeholders and native specialists to identify the LULC classes. Figure 2. displays a flowchart that details the study methodology. To guarantee that the radiance values are precise and constant across various images, the calibration process adjusts for sensor-specific properties, including gain, offset, and responsiveness [24-25]. through Equation (1)

$$L=G\cdot DN+O \quad (1)$$

Where L is the calibrated radiance, G is the sensor gain, O is the sensor offset, and the digital number (DN) that the sensor recorded. After that, the brightness is transformed into top-of-atmosphere (TOA) [26]. after this conversion [26]. Equation-based reflectance (2): Reflectance calibration involves correcting for atmospheric effects, such as absorption and scattering, to obtain accurate surface reflectance values.

$$\rho_\lambda = \frac{\pi L_\lambda d^2}{ESUN\lambda^{sin\theta}} \quad (2)$$

Where ρλ is the surface reflectance. Lλ is the radiance in units of W/(m2 * sr * µm); Watts (W)- This is the unit of power, square meter (m2)- This is the unit of the area, Steradian (sr)- This is the unit of solid angle, micrometer (µm)- This is the unit of wavelength. d is the Earth-sun distance, measured in astronomical units. ESUNλ is the solar irradiance in units of W/(m2 * µm), and Θ is the solar elevation angle in degrees. After the TOA reflectance, the brightness temperatures are calculated (in Kelvin) [26-27] using equation (3) and computed as follows: The relationship between temperature and brightness in remote sensing is often expressed by the Stefan-Boltzmann Law:

$$B=\sigma \cdot T4 \quad (3)$$

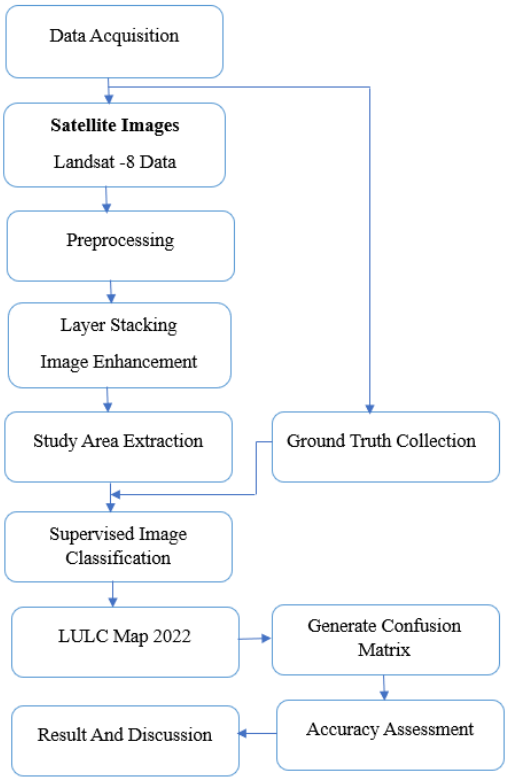

Figure 2. LULC Methodology for the Study Area

4.2 Machine Learning Classifiers

Supervised classification can be done in a number of ways, including with the Support Vector Machine, Maximum Likelihood Classifier, Minimum Distance Classifier, and Mahalanobis Distance Classifier [28].

4.2.1 Maximum Likelihood

The maximum likelihood classification method determines the probability that a given pixel belongs to a specific class by assuming that the statistics for each class in each band are normally distributed [29]. All pixels are classified unless you choose a probability threshold. The class with the highest probability is allocated to each pixel [30]. A pixel is not classified if its highest probability is less than a threshold that you set.

$$D=\ln(ac)\ [0.5\ln(Covc)] + [0.5(X-Mc)\ T(Covc-1)\ (X-Mc)] \quad (1)$$

The variables in this equation are D (the weighted distance), c (a specific class), X (the candidate pixel's measurement vector), Mc (the mean vector of the class c sample), and T (the transposition function). ac (which is either entered based on previous knowledge or defaults to 1.0) represents the percent probability that every potential pixel is a member of class C. The covariance matrix of the class c sample's pixels is called Covc, along with its determinant and inverse, ln, and the natural logarithm function [31].

4.2.2 Mahalanobis Distance

The Mahalanobis distance statistic uses the precision matrix to calculate the distance while accounting for a correlation with the data. During studies, the Mahalanobis Distance is employed for spectrum matching, outlier detection when predicting or calibrating, and model extrapolation detection [32]. Equation 2 shows creating the variance-covariance matrix C is the first step towards computing the Mahalanobis distance [33]. Mahalanobis distance is defined as:

$$MD_i = \sqrt{(x_i - x)C_x^{-1}(x_i - x)^T} \quad (2)$$

where X is the data matrix with n items measured for each of the p variables in the rows. The column-cantered data matrix is denoted by X [34].

4.2.3 Support Vector Machine

SVM is a supervised machine learning approach used for regression and classification issues [35]. SVM classifies data by identifying the hyperplane that divides the data into the most distinct classes. In order to increase the model's generalizability, the hyperplane is selected to maximize the margin between the classes [36-37]. By utilizing a technique known as a "kernel trick," SVM is able to handle both linear and non-linear correlations between characteristics and the target variable [38]. Finding a hyperplane that can divide the classes is made simpler by SVM's ability to turn the input information into an area with more dimensions thanks to the kernel function [39].

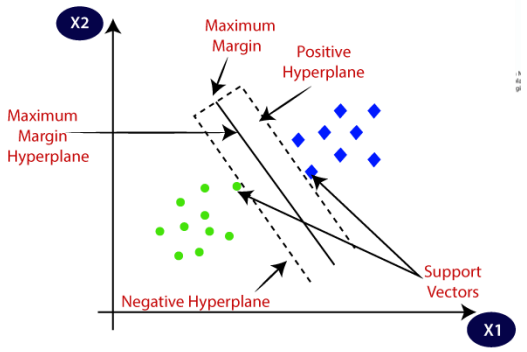

Figure 3. Support vector machine

There are several kinds of kernels that can be used in SVM, each suitable for different types of data distributions. Here are some common kernel types:

1. Linear Kernel:

Formula: $K(x_i, x_j) = x_i^T x_j$

Data that can be separated linearly is used. The decision boundary is a straight line [40].

1. Polynomial Kernel:

Formula: $K(x_i, xj) = (gx_i^T x_j + r)^d, g > 0$.

It is used for non-linear data. The degree *d* and the constant term r are hyperparameters [39].

1. Radial Basis Function (RBF) or Gaussian Kernel-

Formula: $K(x_i, xj) = \exp(-g||x_i - x_j||^2), g > 0$

It is commonly used for non-linear data. The parameter *g* determines the spread of the kernel [40].

1. Sigmoid Kernel-

Formula: $K(x_i, xj) = \tanh(gx_i^T x_j + r)$

It is suitable for information that cannot be divided linearly and can be used in neural network applications [41].

4.2.4 Minimum Distance Classification

Minimum distance classification is used in multi-feature space to place unknown picture data into classes based on how close the image data is to the class. As an index of similarity, the distance is defined as the sum of the minimum and maximum distances. This method involves finding the mean point in digital parameter space for pixels belonging to known classes. Then, when digital number values of the various bands are plotted, unknown pixels are allocated to the class that is arithmetically closest [42]. In order to categorize the research area, a ROI was created for each of the following five primary classes- built-up areas, barren land, dark green vegetation, and green vegetation with water bodies.

5. ACCURACY ASSESSMENT

The statistical findings obtained from the accuracy evaluation approaches are utilized to confirm the precision of the categorization outcome [43]. It is a crucial process since it helps with the error analysis of each class to determine the categorized map's overall dependability [42]. Accuracy evaluation starts with a confusion matrix, sometimes referred to as an error matrix. It compares the categorized image with known reference data that is regarded as correct. Both the total accuracy and the kappa coefficient are evaluated in order to make the forecast. These values are computed using a confusion matrix [44].

A crucial strategy for confirming how effectively the classification captured reality and guaranteeing the correctness of the data obtained from LULC maps was to provide quantitative claims on accuracy evaluation for the classification procedures [45]. To assess how the reference data that were used and the final categorized LULC maps related to each other, confusion matrices were calculated. Confusion matrices, which provide information regarding producer accuracy or mistakes of omission (% of a particular LULC class on the ground that is correctly classified) and user accuracy or errors of commission, are one of the most-often-used techniques to assess the overall classification accuracy [44,46]. The following formula [47]. Equation 1 is used to calculate the percentage of total accuracy:

$$OverallAccuracy(\%) = \frac{TotalNo.ofCorrectedSample}{TotalNo.ofSample} * 100 \quad (1)$$

The following formula, when simplified, equation 2, is used to determine the Kappa coefficient for each of the several categorization algorithms [45,48].

$$Kappa = \frac{P(A)-P(E)}{1-P(E)} \quad (2)$$

where P(A) is the observed accuracy and P(E) is the chance agreement.

The producer accuracy and user accuracy of a classification model. Here's how they are calculated:

Producer accuracy measures how well a certain class has been classified from the perspective of the class (i.e., how many of the actual features of a class are correctly identified).

$$ProducerAccuracy(PA) = \frac{Numberofcorrectlyclassifiedpixelsforagivenclass}{Totalnumberofactualpixelsinthatclass} \times 100 \quad (3)$$

The user accuracy measures the reliability of classification, from the perspective of the user of classification (i.e., how many of the pixels classified as a certain class are actually correct).

$$UserAccuracy(UA) = \frac{Numberofcorrectlyclassifiedpixelsforagivenclass}{Totalnumberofpixelsclassifiedasthatclass} \times 100 \quad (4)$$

6. RESULT

Four distinct classifiers using four SVM kernel types have been used to complete the LULC classification and an overall accuracy comparison for the LULC type, as shown in Table 3 below. Since the Landsat image was obtained on September 22, 2022, the outcomes of two suggested procedures could be compared. MLC Achieved an overall accuracy of 98.99%, with notable confusion

between urban and barren land classes. Linear Kernel for SVM- The overall accuracy of 99.18%, with good separation of vegetation types. Polynomial kernel- Achieved 99.11%, slightly better than the linear kernel. RBF Kernel- The highest accuracy at 99.11%, effectively distinguishing complex LULC classes. Sigmoid Kernel- 95.50% accuracy; struggled slightly with mixed pixels. MHC Recorded an accuracy of 97.83%, effectively differentiating water bodies, but struggled with urban areas. The MDC Lowest accuracy at 93.45%, significant misclassification in densely vegetated regions. Kappa Coefficient also done, MLC-0.98, MHC- 0.96, MDC- 0.91 with users and producer accuracy in Table 3. And SVM-linear (0.98), polynomial (0.98), RBF (0.98), sigmoid (0.98) with users and producer accuracy in Table 4.

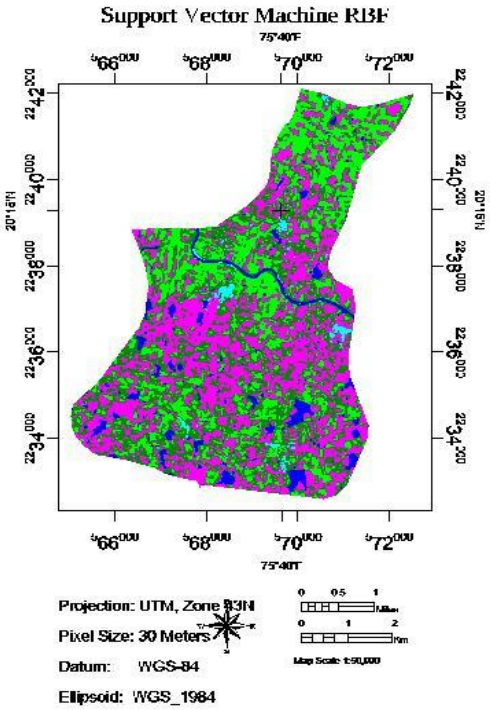

Figure 4. (a)

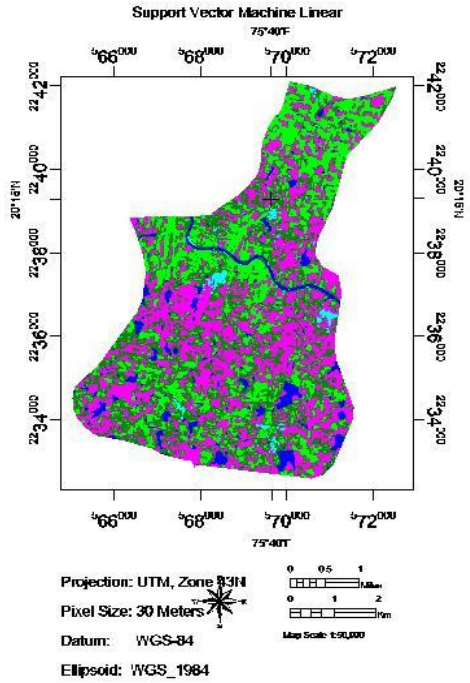

Figure 4. (b)

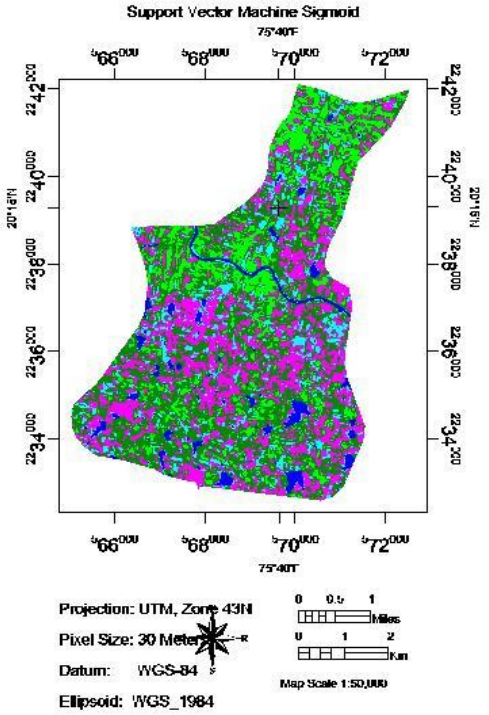

Figure 4. (c)

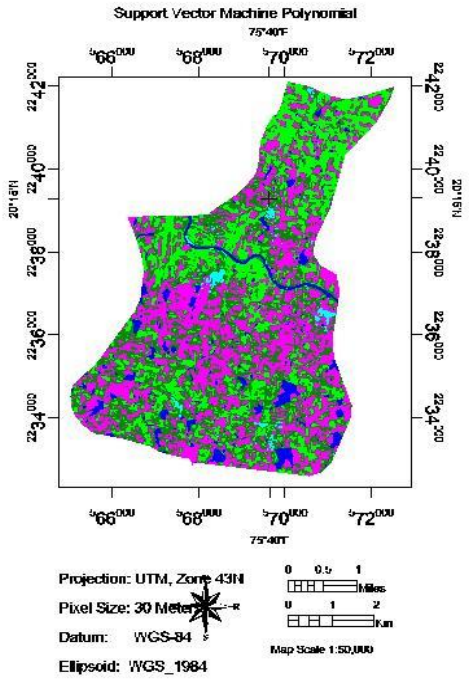

Figure 4. (d)

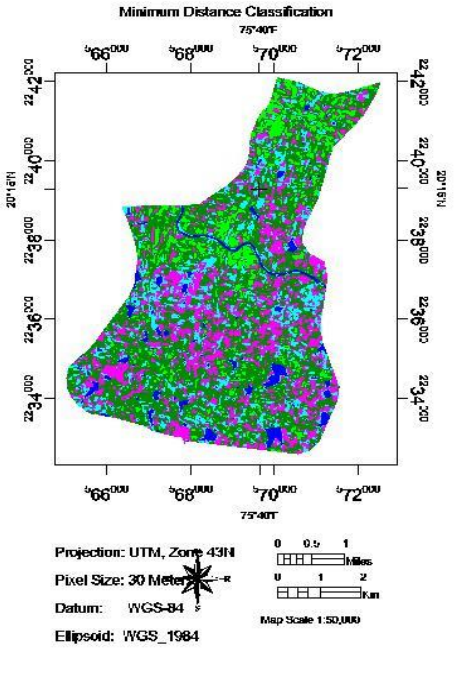

Figure 4. (f)

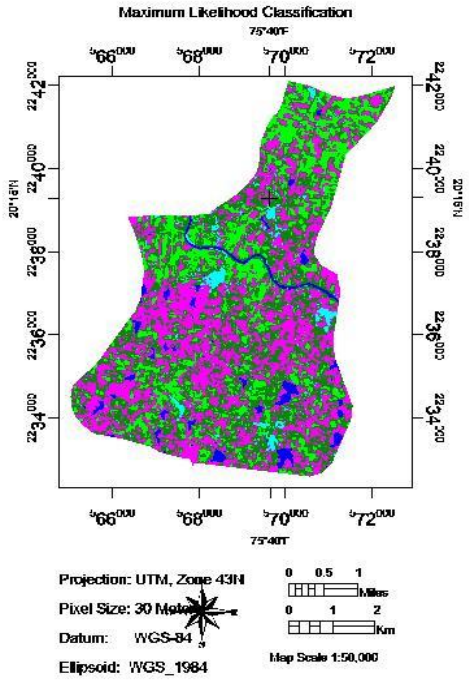

Figure 4. (e)

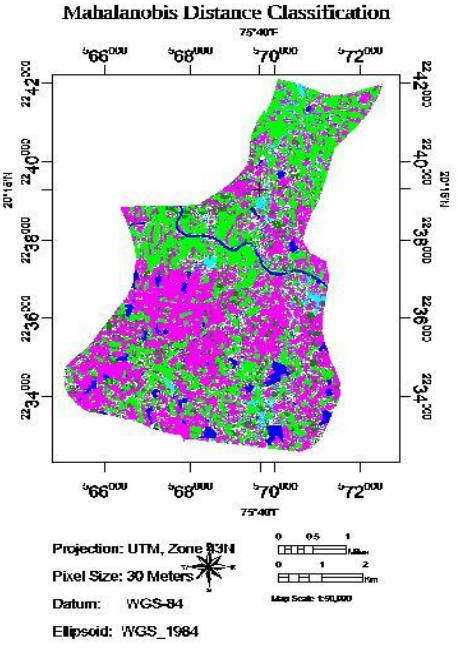

Figure 4. (g)

Figure 4. (h) Legends for Figure 4 (a,b,c,d,e,f,g) respectively.

Figure 4. LULC classification results using SVM classifier with all kernel function (a, b, c, d), maximum Likelihood (e), Mahalnobies Distance classifier(f), Minimum Distance classifier (g).

Also seen all above figure latitude and longitude value around and other specification such as projection, datum, ellipsoid, along with scale.

Table 3. The result of Classification Methods

Classification Methods	Result Discussion (%)	Kappa Coefficient	Producer Accuracy (%)	Users Accuracy (%)
Minimum Distance	93.4728	0.9100	76.71	72.40
Maximum Likelihood	98.9861	0.9859	82.38	81.31
Mahalanobis distance	97.8311	0.9697	82.38	81.31

Table 4. The result of Classification Methods

Classification Methods				
Support Vector Machine (%)	**Linear**	**Polynomial**	**RBF**	**Sigmoid**
	99.17	99.11	99.11	95.50
Kappa Coefficient	0.9885	0.9877	0.9877	0.9373
Producer Accuracy (%)	82.20	82.15	82.06	76.06
Users Accuracy (%)	82.02	81.91	81.97	75.65

6.1 Comparisons the Given Classifiers

Our validation results showed that, for both sets of satellite data, SVM produced LULC maps with generally higher accuracy. The comparison of the algorithms' overall accuracy for Landsat-8 image is shown in Figure 4. The SVM algorithm performed best in terms of overall accuracy and the best tuning parameter, with overall accuracies of 99.17%, 99.11%, 99.11%, and 95.50% for Landsat-8, accordingly Table 2. The various outcomes from other categorization algorithms are also displayed in Figure 5. MLC came in second place with an overall accuracy of 98.98%, behind SVM. The MHC and MDC algorithms came in third and fourth, respectively, with accuracies of 97.83% and 93.47%, with MDC having the worst performance.

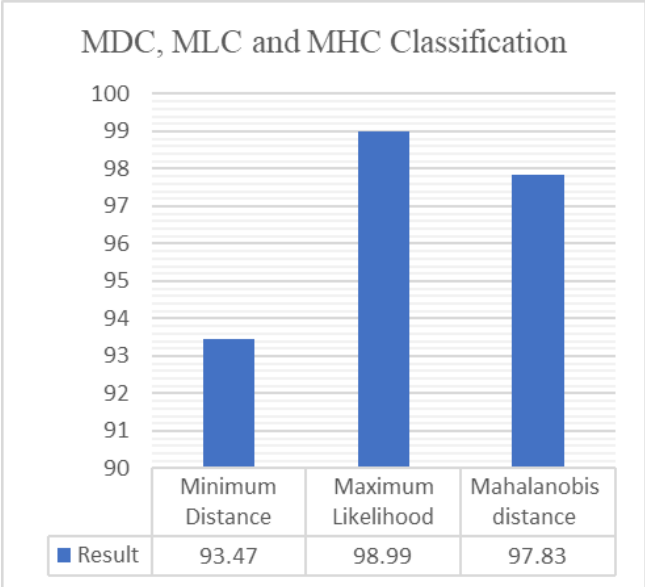

Figure 5. (a)

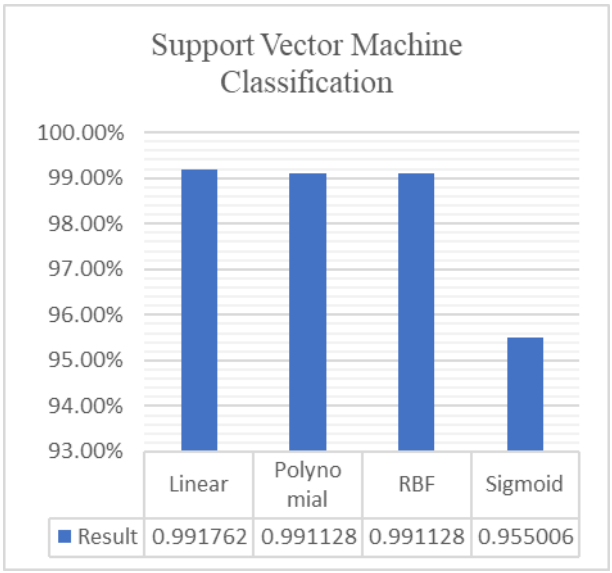

Figure 5. (b)

Figure 5 (a, b). Comparison of Machine Learning Techniques

7. DISCUSSION

SVM with an RBF kernel outperformed other algorithms, demonstrating its capability to handle complex class boundaries and high-dimensional data. MLC provided good results but was less effective in areas with high spectral overlap. MHC performed well in areas with distinct class separations but had limitations in

mixed land cover types. MDC was computationally efficient but had lower classification accuracy, particularly in heterogeneous landscapes.

The superior performance of SVM with a linear kernel is consistent with recent studies highlighting its effectiveness in LULC classification. The performance of MLC aligns with historical data but underscores the improvements possible with advanced machine learning techniques.

Land Use Land Cover (LULC) analysis using Landsat-8 data faces several limitations for a selected study area, including its moderate spatial resolution of 30 meters, which may miss fine-scale details, and its 16-day revisit time, which might not capture rapid changes. Cloud cover and atmospheric conditions can obscure images, while spectral limitations can lead to misclassification of similar land cover types. Data processing requires advanced technical expertise and significant computational resources. Temporal gaps, mixed pixels, and terrain-induced geometric distortions can further complicate analysis. Additionally, managing the large data volume and associated processing costs can be challenging, necessitating complementary data, sources, and advanced techniques to improve accuracy. While pixel-based classification, which often resulted in higher rates of misclassification due to the mixed pixel problem.

In future work, we aim to enhance Land Use Land Cover (LULC) analysis by utilizing high-resolution and frequent satellite imagery, integrating data from diverse sources such as multispectral, hyperspectral, LiDAR, and SAR sensors. We plan to apply advanced machine learning techniques, including deep learning and transfer learning, to improve classification accuracy and automation. Additionally, leveraging cloud computing and big data platforms will enable scalable and real-time monitoring. We will also explore the integration of LULC data with socio-economic datasets to support policy-making and sustainable development. Future research will focus on developing improved change detection methods and creating user-friendly tools to facilitate broader application and collaboration.

The limitation of the study lies in its focus on a single year of data (2022), which restricts the ability to perform comprehensive change detection over time. Without multiple temporal data points, the study can only provide a snapshot of land cover at that particular time, limiting the analysis of long-term trends or dynamic shifts in LULC caused by human activities or natural processes.

8. CONCLUSION

The conclusion from the above results is that the Support Vector Machine (SVM) with four different kernels-linear, radial basis function (RBF), sigmoid, and polynomial-demonstrated the highest accuracy in classifying land use land cover (LULC) compared to other classifiers. When compared to four other machine learning techniques, the experimental findings further demonstrated the superiority of the SVM for LULC classification. In addition, SVM using a radial kernel performs noticeably better than another kernel when it comes to classifying land cover. Subsequent research endeavors may enhance the classification accuracy by assessing water bodies and green vegetation using seasonal data sets and integrating them with diverse data sets. Including the Minimum Distance Classifier (MDC), Maximum Likelihood Classifier (MLC), and Mahalanobis Distance Classifier (MHC). The study highlights the effectiveness of SVM in providing precise and reliable LULC classification, which is crucial for informed decision-making in land management, sustainable development, and resource utilization. Additionally, research underscores the importance of integrating advanced classification methods and Geographic Information Systems (GIS) and Remote Sensing (RS) for accurate mapping and long-term monitoring of land cover changes.

Acknowledgement

The authors would like to acknowledge Landsat-8 imagery from U.S. Geological Survey (USGS).

Author contributions

Pratibha P. Dapke contributed to the conceptualization, data collection, satellite imagery processing, analysis, manuscript editing, critical review and manuscript writing. **Syed Ahteshamuddin Quadri, Samadhan M. Nagare, Sagar B. Bandal Manasi R. Baheti** was responsible for supervision, critical review, manuscript editing and granted final approval for manuscript submission.

Conflicts of interest

The authors declare no conflicts of interest.

REFERENCES

1. Mariye, M., Jianhua, L., & Maryo, M. (2023). Land use land cover change analysis and detection of its drivers using geospatial techniques: a case of south-central Ethiopia. 34(1), 309–332. https://doi.org/https://doi.org/10.1080/27669645.2022.2139023
2. Digra, M., Dhir, R., & Sharma, N. (2022). Land use land cover classification of remote sensing images based on the deep learning approaches: a statistical analysis and review. 15(1003). https://doi.org/https://doi.org/10.1007/s12517-022-10246-8
3. Twisa, S., & Buchroithner, M. F. (2019). Land-Use and Land-Cover (LULC) Change Detection in WamiRiver Basin, Tanzania. 8, 136. https://doi.org/doi:10.3390/land8090136
4. Zhang, C., & Li, X. (2022). Land Use and Land Cover Mapping in the Era of Big Data. 11, 1692. https://doi.org/10.3390/land11101692
5. Ahmed, M., Prince, H. M., & Shafri, H. Z. (2019). Landuse/Landcover mapping and monitoring using Remote sensing and GIS with environmental integration. 357, 012038. https://doi.org/doi:10.1088/1755-1315/357/1/012038

6. Azizi, P., Soltani, A., Bagheri, F., Sharifi, S., & Mikaeili, M. (2022). An Integrated Modelling Approach to Urban Growth and Land Use/Cover Change. 11, 1715. https://doi.org/10.3390/land11101715
7. Vivekananda, G., Swathi, R., & Sujith, A. (2021). Multi-temporal image analysis for LULC classification and change detection. 54(S2), 189–199. https://doi.org/https://doi.org/10.1080/22797254.2020.1771215
8. Zhu, K., Cheng, Y., Zang, W., Kabil, M., Zhou, Q., Archi, Y. E., Dávid, L. D. (2023). Multiscenario Simulation of Land-Use Change in Hubei Province, China Based on the Markov-FLUS Model. 12(744). https://doi.org/10.3390/land12040744
9. Indraja, G., Aashi, A., & Vema, V. K. (2024). Spatial and temporal classification and prediction of LULC in Brahmani and Baitarni basin using integrated cellular automata models. 196(117). https://doi.org/https://doi.org/10.1007/s10661-023-12289-0
10. Dourbi, G., Kalra, B., & Kumar, S. (2023). Investigating Land Use and Land Cover Classification Using Landsat-8 Remote Sensing Data by Comparing Machine Learning Algorithms (Case Study: Dehradun Region). https://doi.org/10.1007/978-981-99-4577-1_15
11. Jombo, S., & Adelabu, S. (2023). Evaluating Landsat-8, Landsat-9 and Sentinel-2 imageries in land use and land cover (LULC) classification in a heterogeneous urban area. 88(Suppl 1), 377–399https://doi.org/https://doi.org/10.1007/s10708-023-10982-8
12. Shahfahad, M. W. N., Das, T., Talukdar, S., Asgher, M. S., & Rahman, A. (2022). Prediction of land use changes at a metropolitan city using integrated cellular automata: past and future. https://doi.org/https://doi.org/10.1080/24749508.2022.2132010
13. Atlas, M. (2007). The dilemma between development and protection in the mountains of Morocco - the case of parks of the. 82(4).
14. Mohajane, M., Essahlaoui, A., Oudija, F., El Hafyani, M., El Hmaidi, A., El Ouali, A., … Teodoro, A. C. (2018). Land Use/Land Cover (LULC) Using Landsat Data Series (MSS, TM, ETM+ and OLI) in Azrou Forest, in the Central Middle Atlas of Morocco. 5(131). https://doi.org/10.3390/environments51201
15. Mungai, L. M., Messina, J. P., & Zulu, L. C. (2022). Modeling Spatiotemporal Patterns of Land Use/Land Cover Change in Central Malawi Using a Neural Network Model. 14, 3477. https://doi.org/https://doi.org/10.3390/rs14143477
16. Villi, O., & Yakar, M. (2024). Sensortechnologies in unmanned aerial vehicles: types and applications.Advanced UAV, 4(1), 1-18.
17. Villi, Ö., & Yavuz, H. (2024). The utilization of gimbal systems in unmanned aerial vehicles.Advanced UAV, 4(1), 19-30.
18. D'Allestro, P., & Parente, C. (2015). GIS application for NDVI calculation using Landsat-8 OLI images. 10, 42099–42102.
19. Chavez, P. S. J. (1988). An improved dark-object subtraction technique for atmospheric scattering correction of multispectral data. 24, 459–479.
20. Tutorial, A. (2020). ArcGIS Tutorial for Beginners.
21. Navarro-Cerrillo, R. M., Manzanedo, R. D., Bohorque, J., Sánchez, R., Sánchez, J., de Miguel, S., … Palacios, G. (2013). Structure and spatio-temporal dynamics of cedar forests along a management gradient in the Middle Atlas, Morocco. 289, 341–353.
22. Yakar, M., & Dogan, Y. (2019). 3D Reconstruction of Residential Areas with SfM Photogrammetry. In Advances in Remote Sensing and Geo Informatics Applications: Proceedings of the 1st Springer Conference of the Arabian Journal of Geosciences (CAJG-1), Tunisia 2018 (pp. 73-75). Springer International Publishing
23. Atak, B., Varlık, A., Güngör, R., & Yılmaz, S. O.(2024). Unmanned aerial vehicle (UAV)-based cadastral mapping accuracy analysis: a case study of Sarayköy, Konya.Advanced UAV, 4(1), 31-41.
24. Schroeder, T. A., Cohen, W. B., Song, C., Canty, M. J., & Yang, Z. (2006). Radiometric correction of multi-temporal Landsat data for characterization of early successional forest patterns in Western Oregon. 103, 16–26.
25. Tan, K. C., Lim, S., MatJafri, M. Z., & Abdullah, K. (2010). Landsat data to evaluate urban expansion and determine land use/land cover changes in Penang Island, Malaysia. 60, 1509–1521.
26. Giannini, M. B., Belfiore, O. R., Parente, C., & Santamaria, R. (2015). Land Surface Temperature from Landsat 5 TM Images: Comparison of Different Methods Using Airborne Thermal Data. 8, 83–90.
27. Unel, F. B., Kusak, L., & Yakar, M. (2023). GeoValueIndex map of public property assets generating via Analytic Hierarchy Process and Geographic Information System for Mass Appraisal: GeoValueIndex. Aestimum, 82, 51-69.
28. Ghayour, L., & Neshat, A. (2021). Performance Evaluation of Sentinel-2 and Landsat-8 OLI Data for Land Cover/Use Classification Using a Comparison between Machine Learning Algorithms. 13, 1349. https://doi.org/https://doi.org/10.3390/rs13071349
29. Strahler, A. H. (1980). The use of prior probabilities in maximum likelihood classification of remotely-sensed data. 10, 135–163.
30. Matkar, P. S., & Zende, A. M. (2017). Land Use/Land Cover Changes Pattern Using Geospatial Techniques - Satara District, Maharashtra, India: A Case Study.
31. Thomas, I. L., Benning, V. M., & Ching, N. P. (1987). Classification of Remotely-Sensed Images.
32. Nagne, A. D., Dhumal, R. K., Vibhute, A. D., Rajendra, Y. D., Gaikwad, S., Kale, K. V., & Mehrotra, C. (2017). Performance Evaluation of Urban Areas Land Use classification from Hyperspectral Data by Using Mahalanobis classifier.
33. Polat, N., & Kaya, Y. (2021). Investigation of the Performance of Different Pixel-Based Classification Methods in Land. 3(1), 01–06.
34. De Maesschalck, R., Jouan-Rimbaud, D., & Massart, D. L. (2000). The mahalanobis distance. 50(1), 1–18.

35. Vapnik, V. (1998). The support vector method of function estimation. 55–85.
36. Qian, Y., Zhou, W., Yan, J., Li, W., & Han, L. (2015). Comparing Machine Learning classifiers for object-based land cover classification using very high-resolution imagery. 7(1), 153–168.
37. Noi, T., Phan, & Kappas, M. (2017). Comparison of random forest, k-nearest neighbor, and support vector machine classifiers for land cover classification using Sentinel-2 imagery. 18(1), 18.
38. Pretorius, L., Brown, L. R., Bredenkamp, G. J., & van Huyssteen, C. W. (2016). The ecology and classification of wetland vegetation in the Maputaland Coastal Plain, South Africa. 46(2), 125–139.
39. Avci, C., Budak, M., Yagmur, N., & Bektas Balcik, F. (2023). Comparison between random forest and support vector machine algorithms for LULC classification. 8(1), 01–10.
40. Han, X., Pan, J., & Devlin, A. T. (2018). Remote sensing study of wetlands in the Pearl River Delta during 1995–2015 with the support vector machine method. 12(3), 521–531.
41. Kavzoglu, T., & Colkesen, I. (2009). A kernel functions analysis for support vector machines for land cover classification. 11(5), 352–359.
42. Pal, S., Pandey, S., Sharma, S., & Nair, R. (2022). Land use and land cover classification of Jabalpur district using minimum distance classifier. SP-11(11), 1161–1163.
43. Congalton, R. G. (1991). A Review of Assessing the Accuracy of Classifications of Remotely Sensed Data.37, 35–46. https://doi.org/10.1016/0034-4257(91)90048-B
44. Lillesand, T. M., Kiefer, R. W., & Chipman, J. W. (2004). Remote Sensing and Image Interpretation. 53. https://doi.org/https://doi.org/10.1017/CBO9781107415324.004
45. Gwet, K. (2002). Kappa Statistic Is Not Satisfactory for Assessing the Extent of Agreement between Raters. 1(1), 1–6.
46. Tran, D. X., Pla, F., Latorre-Carmona, P., Myint, S. W., Caetano, M., & Kieu, H. V. (2017). Characterizing the Relationship between Land Use Land Cover Change and Land Surface Temperature. 124, 119–132. https://doi.org/https://doi.org/10.1016/j.isprsjprs.2017.01.001
47. Pal, S., & Ziaul, S. (2016). Detection of Land Use and Land Cover Change and Land Surface Temperature in English Bazar Urban Centre. 20, 125–145. https://doi.org/https://doi.org/10.1016/j.ejrs.2016.11.003
48. Viera, A. J., & Garrett, J. M. (2005). Understanding Interobserver Agreement: The Kappa Statistic. 37, 360–363.